Plasma Sources Science and Technology

PURPOSE-LED PUBLISHING™

LETTER • **OPEN ACCESS**

Streamer–surface interaction in an atmospheric pressure dielectric barrier discharge in argon

To cite this article: Aleksandar P Jovanović *et al* 2022 *Plasma Sources Sci. Technol.* **31** 04LT02

OPEN ACCESS
IOP Publishing

Letters
Plasma Sources Science and Technology

Plasma Sources Sci. Technol. **31** (2022) 04LT02 (8pp)
https://doi.org/10.1088/1361-6595/ac63df

Letter

Streamer–surface interaction in an atmospheric pressure dielectric barrier discharge in argon

Aleksandar P Jovanović*, Detlef Loffhagen and Markus M Becker

Leibniz Institute for Plasma Science and Technology (INP), Felix-Hausdorff-Str. 2, 17489 Greifswald, Germany

E-mail: aleksandar.jovanovic@inp-greifswald.de

Received 7 November 2021, revised 18 March 2022
Accepted for publication 4 April 2022
Published 28 April 2022

Abstract

An atmospheric-pressure dielectric barrier discharge (DBD) in argon is investigated using a time-dependent and spatially two-dimensional fluid-Poisson model in axisymmetric geometry. The focus is on the streamer–surface interaction and the cathode-layer formation during the first discharge event in the single-filament DBD driven by sinusoidal voltage. A characteristic structure consisting of a volume streamer propagating just above the dielectric and simultaneous development of an additional surface discharge near the cathode is observed. The analysis of the electric field, electron production and loss rates, and surface charge density distribution shows that the radial deflection of the volume streamer is driven by free electrons remaining in the volume from the Townsend pre-phase and guided by the radial component of the electric field. The surface discharge occurring between the deflected volume streamer, which acts as virtual anode, and the dielectric surface is governed by ion-induced secondary electron emission and the surface charges accumulated on the dielectric.

Keywords: dielectric barrier discharge, filamentary regime, modelling, argon

(Some figures may appear in colour only in the online journal)

Dielectric barrier discharges (DBDs) are widely used as a source of low-temperature plasmas at atmospheric pressure [1–3]. Due to their importance, they are thoroughly investigated both experimentally [4–12] and by numerical modelling [13–23]. Depending on the operating conditions, DBDs appear either in a diffuse (Townsend or glow-like) mode or as a filamentary discharge, which is governed by the streamer mechanism [3, 24]. The focus of this letter is on the analysis of a filamentary DBD in a single-filament configuration, which is frequently used to geometrically stabilise the plasma filament at the position with the shortest gap between two hemispherical electrodes [7, 11, 12]. In particular, the interaction of the first cathode-directed streamer with the dielectric surface is investigated. The processes occurring during the arrival of the streamer at the cathode, the cathode-layer formation, and the streamer branching at the surface have rarely been studied so far and are far from being completely understood [25]. This also applies to the influence of the streamer–surface interaction on macroscopic quantities such as the electric current, which is likewise part of the present investigations. Previous modelling of filamentary DBDs has usually been carried out using two-dimensional (2D) fluid models, in order to fully describe the development of the constricted discharge channels

* Author to whom any correspondence should be addressed.

and to capture the transient discharge dynamics. The majority of these 2D modelling studies were performed for nitrogen, oxygen, and air-like mixtures, respectively [13–18], and plane-parallel configurations or pin-to-plane geometries were usually used. Furthermore, surface streamers in surface DBDs and coplanar arrangements were investigated in [8, 9, 18, 22, 23, 26–28]. Investigations of volume streamers interacting with dielectric surfaces were presented in [16, 29, 30]. The focus of these analyses was again on air-like mixtures, where the propagation of volume and surface streamers is strongly influenced by photoionisation and photoemission processes [16, 29].

In the present paper, the first breakdown event and the streamer–surface interaction in a single-filament DBD in argon at atmospheric pressure are studied for the first time by means of a time-dependent 2D fluid-Poisson model in axisymmetric geometry. Results of a detailed analysis of the cathode-layer formation and of the appearance of a simultaneous propagation of a volume streamer and development of a secondary surface discharge near the dielectric surface are presented and discussed. Note that such two-fold mechanism and resulting double-layer structure at a streamer–surface interface have not been reported so far. The understanding of the formation of this structure helps grasping the process of transition from volume to surface discharge and particularly the cathode-layer formation in filamentary DBDs. The correlation of the spatiotemporal development of the DBD with global quantities, such as the discharge current, supports the understanding of specific features of these quantities. This can also assist the interpretation of experimental data, which normally cannot resolve the plasma-surface interface in great detail.

The modelling studies are carried out for the asymmetric discharge configuration shown in figure 1. It consists of two hemispherical electrodes with a radius of $R = 2$ mm separated by a gap of $d = 1.5$ mm as described in [11, 19]. The grounded electrode is covered with an alumina layer (thickness: $\Delta = 0.5$ mm, relative permittivity: $\varepsilon_r = 9$). The metallic electrode is powered by a sinusoidal voltage with the amplitude $U_0 = 3$ kV and the frequency $f = 60$ kHz.

The model comprises a set of balance equations for the particle number densities of electrons and the most important argon species, Poisson's equation for the electric potential and field, the electron energy balance equation and a balance equation for the surface charge density. The reaction kinetics model of argon includes the same species and reaction kinetic processes as considered in [31]. Besides the electron component, particle balance equations are solved for atomic (Ar^+) and molecular (Ar_2^+) ions, as well as the lumped excited atomic (Ar^*) and molecular (Ar_2^*) states of argon.

The system of equations is solved in cylindrical coordinates using the commercial software package COMSOL Multiphysics® [32]. For all calculations, the boundary conditions for the balance equations are applied in accordance with [19] and adapted to the 2D description. Specifically, boundary conditions describing the partial reflection of fluxes (equations (9), (11) and (12) in [19]) are imposed for the balance equations at all plasma-facing walls. Here, the balance equations for the particle number density and energy density

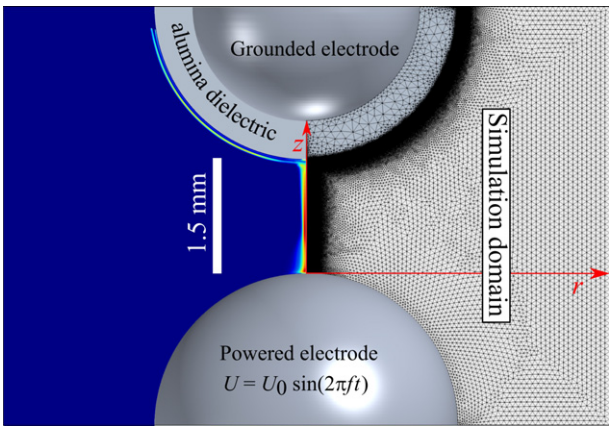

Figure 1. Illustration of the discharge in a single-filament configuration set-up, simulation domain and computational mesh.

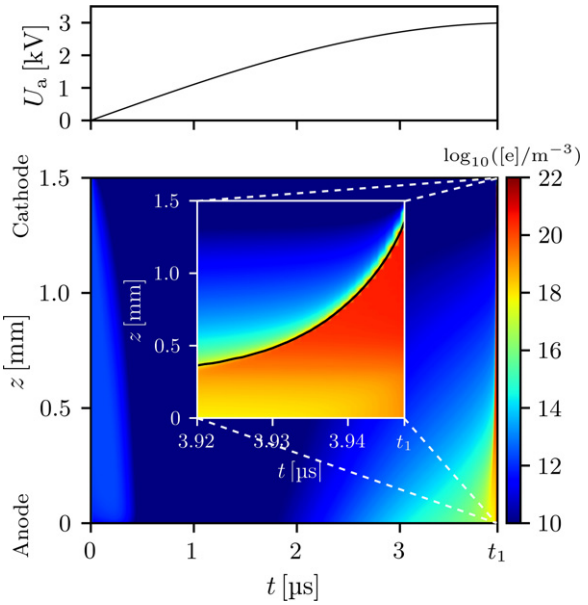

Figure 2. Temporal variation of the applied voltage (top) and spatiotemporal evolution of the electron number density during the Townsend pre-phase and streamer propagation phase (bottom). The inset zooms into the streamer propagation phase. The time t_1 denotes the instant of streamer arrival at the cathode. Note that the lower boundary of the colour bar is set to 10^{10} m^{-3} to highlight important discharge features. The minimum of the electron number density is 1.65×10^7 m^{-3} in this time range.

of electrons contain an additional term describing the ion-induced emission of secondary electrons. The same values for the reflection and secondary electron emission coefficients as in [19] are used. Since the focus here is on the initial discharge with clean and uncharged surfaces, no photo processes such as photodesorption are taken into account in the model. The Poisson equation is complemented by equation (15) in [19] describing the effect of surface charges on the electric field at the alumina covered grounded electrode, where equation (17) in [19] is used to calculate the surface charge density. The prescribed electric potential is applied as boundary condition for Poisson's equation at the metal electrode. Zero-flux boundary conditions imposed at the outer boundaries of the computational domain do not affect the presented results. Assuming

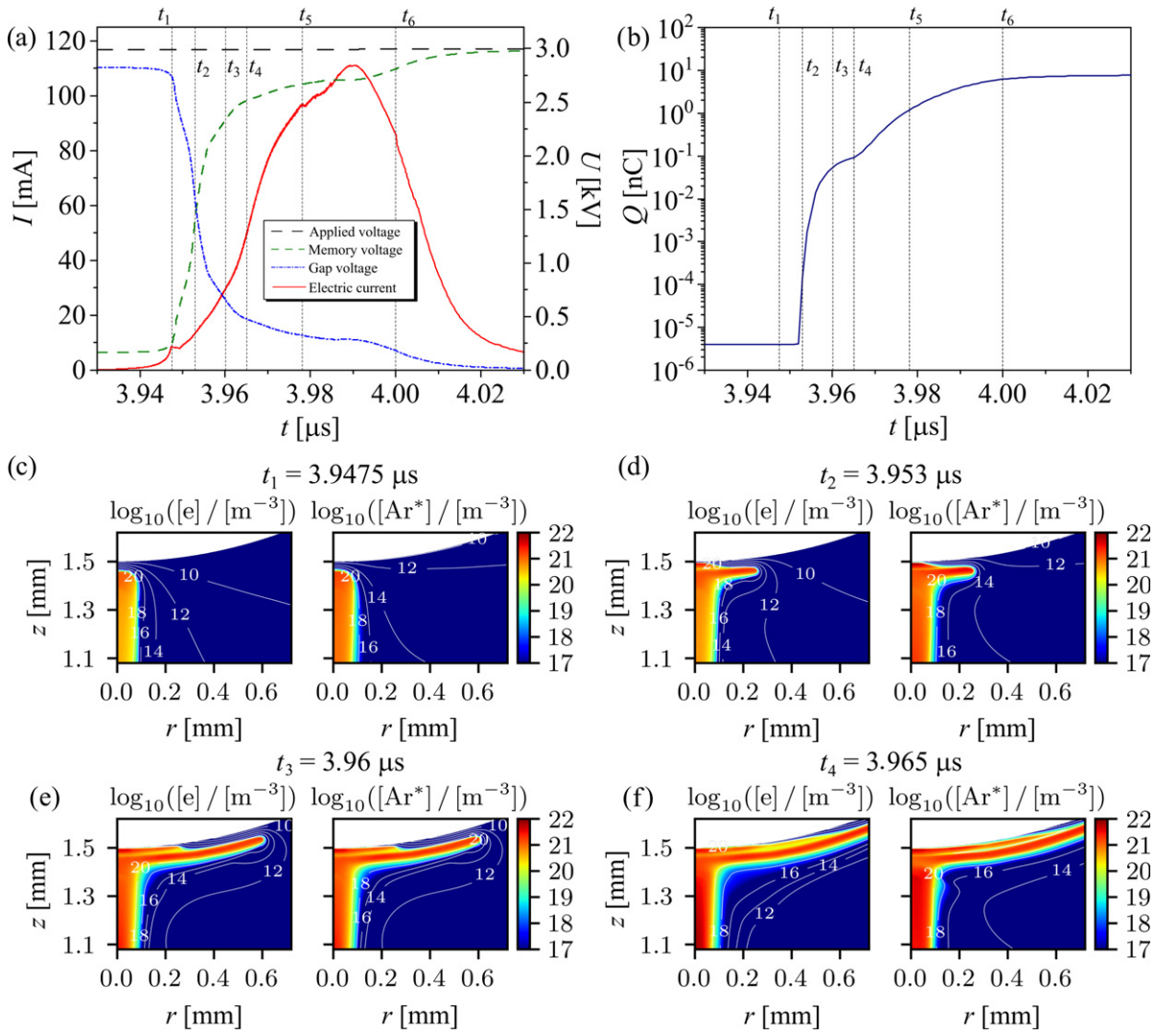

Figure 3. Results of DBD modelling showing the temporal variation of the electric current, applied voltage, gap voltage and memory voltage (a), the temporal variation of the surface charge deposited on the dielectric surface (b), as well as the spatial profiles of electron and Ar^* number densities for the characteristic times t_1–t_4 (c)–(f).

quasi-neutrality, the number densities of excited species and ions of argon are initially set to 10^{12} m^{-3}, the initial number density of electrons is set to 2×10^{12} m^{-3}, and the initial mean electron energy is assumed to be 3 eV in the entire solution domain. The electric current is calculated as the surface integral of the total current density at the metal anode surface.

It should be stressed out that the particular axisymmetric fluid model is chosen due to its computational efficiency. The model accurately describes the discharge inception and streamer propagation between the electrodes. Some quantities, such as the current, might be overestimated due to the assumed axial symmetry. During the cathode layer formation, the electric field might reach excessively large values for a short time, which could also influence the accuracy of the model. Nonetheless, the present model can still provide valuable insight into the processes occurring during the movement of the streamer near and its interaction with the surface. A fully three-dimensional (3D) model involving stochastic effects is required to take into account possible branching of streamer channels covering the curved electrodes. However, such 3D model requires enormous computing power and the available computer architecture is a limiting factor.

Figure 2 exhibits the applied voltage in conjunction with the spatiotemporal evolution of the electron number density along the symmetry axis z at radial position $r = 0$. The represented time interval ranges from $t = 0$ until the end of the volume streamer propagation phase ($t = t_1$). With increase of the applied voltage the initial electrons drift towards the anode and the electron density drops below 10^{10} m^{-3}. Note that due to these initial transport losses the evolution of discharge inception and breakdown is hardly influenced by the assumed initial particle number densities. As the voltage further increases, the flux of ions to the cathode becomes important by providing initial electrons via secondary electron emission. When these electrons gain enough energy to ionise the gas, the Townsend pre-phase is initiated. With this, the electron density gradually rises over time with an exponential increase from the cathode towards the anode. This leads to the inception of the positive (cathode-directed) streamer at $t \approx 3.9$ μs (cf inset of figure 2). Its propagation is driven by direct ionisation of argon atoms in

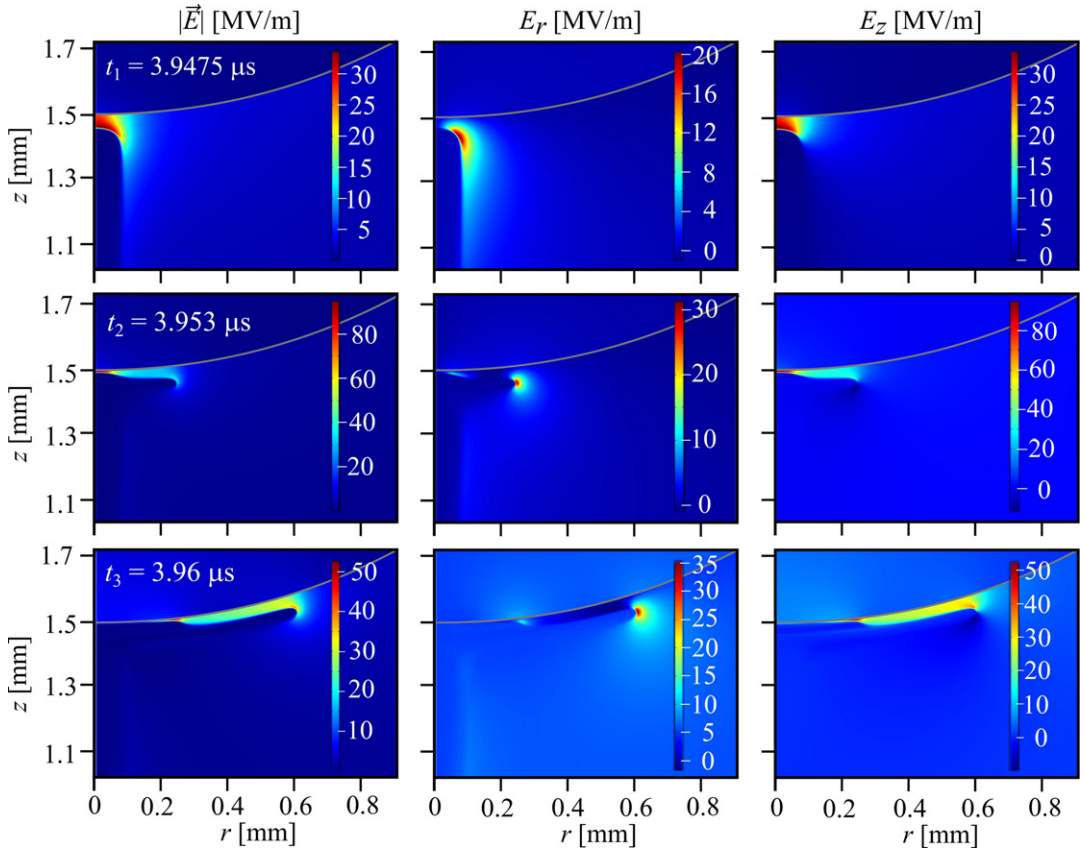

Figure 4. Spatial distribution of the magnitude $|\vec{E}|$ (left column), radial component E_r (middle column) and axial component E_z (right column) of the electric field at characteristic times t_1–t_3 introduced in figure 3(a).

collisions with electrons and the streamer continuously accelerates from velocities of about 10^4 m s^{-1} to roughly 10^5 m s^{-1} when approaching the cathode. These values are in excellent agreement with experimental results for the velocity of a positive streamer in a symmetric atmospheric-pressure argon DBD under similar conditions (gap of 1 mm, voltage amplitude of about 2 kV, and frequency of 5.2 kHz) [33].

Figure 3 presents (a) the temporal evolution of the electric current I, the applied voltage U_a, the gap voltage U_g, the memory voltage $U_m = U_a - U_g$ and (b) the accumulated surface charge Q, as well as (c)–(f) the spatial distribution of the number density of electrons and excited argon atoms at times t_1–t_4. These times correspond to the arrival of the volume streamer at the cathode surface (t_1) and different moments of the cathode-layer formation phase (t_2–t_4). Here, it is important to note that the gap voltage is calculated as the potential drop across the gap at radial position $r = 0$.

During the streamer propagation phase ($t \leqslant t_1$), the electric current steeply increases and reaches a local maximum at $t = t_1$, while the gap and memory voltages remain almost constant in this time range (cf figure 3). A similar current shape was observed in [34–36]. According to [34, 35] and in agreement with the present results, the local current maximum is attributed to the streamer arrival at the cathode and is caused by the displacement current due to the reconfiguration of the electric field. It should be noted that this feature (local current maximum) is the result of a continuous process of balancing electron production and losses (see below), which leads to slowing down and eventual stopping of the streamer propagation. In figure 3(c) it can be seen that at time t_1 a thin gap of about 40 µm with small electron density is formed between the streamer head and the dielectric boundary. In the time range t_1–t_2 the volume streamer is deflected and continues propagating along the surface (cf figure 3(d)). At the same time, the ion-induced emission of secondary electrons causes a secondary breakdown in the gap between the streamer head acting as a virtual anode and the dielectric cathode. With this, the surface charges start to accumulate on the dielectric surface (cf figure 3(b)), which is accompanied by a steep increase of the memory voltage and corresponding drop of the gap voltage as well as a further rise of the electric current (cf figure 3(a)). In the time range t_2–t_4, a surface discharge starts to propagate in the gap between the radially propagating volume streamer and the dielectric surface (cf figures 3(d)–(f)). Note that the double-layer structure caused by the deflected volume streamer and the secondary discharge in the sheath region shows similarities with the observation of Sharma *et al* [27] for a surface DBD in argon, where the splitting of a surface streamer into a surface branch and a volume branch results in a similar structure near the dielectric surface.

With ongoing coverage of the surface by the discharge, the accumulated surface charge increases further. This finally leads to a drop of the electric field and initiation of the decay

phase as described, e.g. in [18]. The maximum current is reached at about 70 ns after streamer initiation and 42 ns after the arrival of the streamer at the cathode (cf figure 3(a)).

When looking at the spatial profiles of the excited argon atoms shown in figures 3(c)–(f), it becomes obvious that they closely follow the behaviour of the electrons. The radial distribution of Ar^* is a bit more broadened than that of the electrons because of the lower energy threshold for electron-impact excitation compared to the ionisation of argon.

In order to determine the reason for the volume streamer deflection and the appearance of the surface discharge, the electric field $\vec{E}$ is analysed in figure 4. It shows the spatial distribution of the magnitude $|\vec{E}|$ (left column), radial component E_r (middle column) and axial component E_z (right column) for the characteristic times t_1–t_3. From the spatial profiles of the electric field at t_1 it can be seen that E_r becomes of the same order of magnitude as E_z when the volume streamer approaches the cathode. This is caused by the broadening of the streamer head when approaching the dielectric and affects the further streamer development. Namely, the requirements for streamer propagation are the existence of free electrons in front of the streamer and the specific configuration of the electric field directing these electrons towards the streamer head [18]. As the number of free electrons in front of the streamer drops due to the shrinking space in front of it, the propagation slows down and eventually stops independently of the magnitude of the axial component of the electric field. However, free electrons in the volume near the streamer head resulting from the Townsend pre-phase (cf contour lines in figure 3(c)) and the high radial electric field provide the conditions for continuation of the streamer propagation in radial direction (cf t_2–t_3 in figure 4). It should be stressed that this happens before the ions produced during the streamer phase are able to reach the surface and induce the excessive emission of secondary electrons. Although photo processes play an important role in air-like gases [16–18], in the argon plasma considered here, they are not expected to have an impact on the discharge as an additional electron source. Therefore, surface processes do not affect the deflection and further propagation of the volume streamer.

Simultaneously to the deflection of the volume streamer, the cathode layer is formed in the narrow region just in front of the cathode surface (cf t_2 in figure 4). Due to the increase of space charge density and the drastic reduction of the cathode sheath to about 6 µm, the magnitude of the electric field reaches a maximum value of about 95 MV m^{-1} in front of the cathode surface for a few nanoseconds around t_2. This corresponds to a reduced electric field of about 3900 Td, where 1 Td = 10^{-21} Vm^2. This large electric field causes the onset of the surface discharge, which starts to propagate just above the cathode surface. Note that the surface discharge contributes to the charge accumulation much more than the deflected volume streamer, which continues to propagate about 30 µm in front of the dielectric surface.

Figure 5 explains how the reconfiguration of the electric field at arrival of the streamer at the cathode and the amplification of the radial field component causes the deflection of the volume streamer. The axial cut ($r = 0$) of the electron source

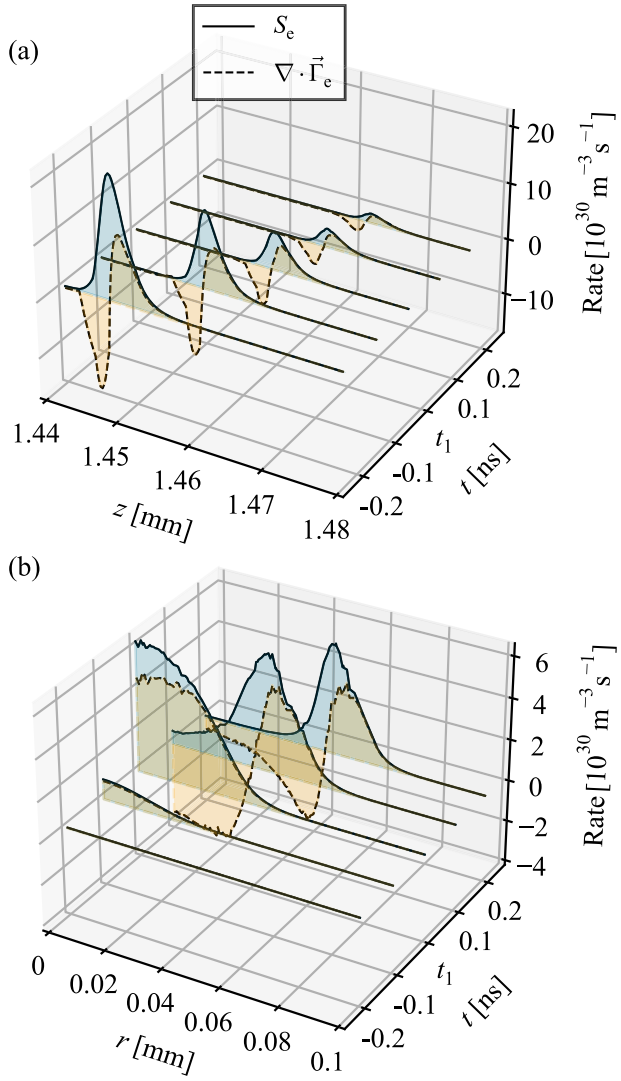

Figure 5. Electron source term S_e (blue-shaded surface) and divergence of the electron flux $\nabla \cdot \vec{\Gamma}_e$ (orange-shaded surface) at the head of the volume streamer in axial ($r = 0$) (a) and radial ($z =$ 1.46 mm) (b) direction at times $t_1 \pm 0.1$ ns and $t_1 \pm 0.2$ ns, i.e. at the moment of streamer arrival at the cathode.

term S_e and the divergence of the electron flux $\nabla \cdot \vec{\Gamma}_e$ shown in figure 5(a) for times shortly before ($t = t_1 - 0.2$ ns and $t = t_1 - 0.1$ ns) and after ($t = t_1 + 0.1$ ns and $t = t_1 + 0.2$ ns) the moment of the streamer arrival at the cathode surface ($t = t_1$) exhibit a decreasing tendency of these quantities over time. At $t = t_1 - 0.2$ ns, the electron production rate is much higher than the transport loss rate and a significant gain of electrons due to transport can be observed behind the ionisation front. At $t = t_1 - 0.1$ ns, both rates keep decreasing and become more balanced. A similar tendency can be observed at $t = t_1$ and $t = t_1 + 0.1$ ns, noting that the movement of the ionisation front slows down. At $t = t_1 + 0.2$ ns, the production and the loss of electrons at the axis balance each other out. This leads to the cessation of the streamer propagation along the discharge axis near $z = 1.46$ mm.

At the same time, the variation of the rates in radial direction is opposite to that in axial direction (cf figure 5(b)). At $t = t_1 -$ 0.2 ns the electron source term as well as the divergence of the

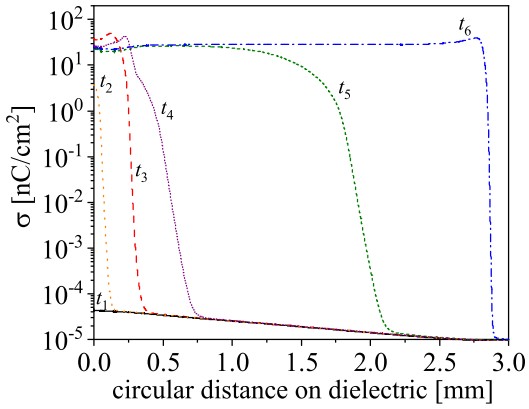

Figure 6. Spatial distribution of the surface charge density σ on the dielectric surface for the characteristic times t_1–t_6.

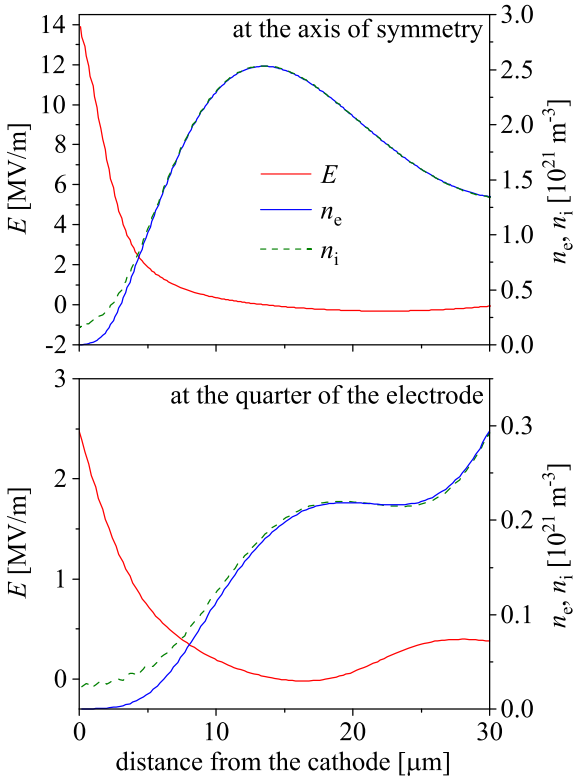

Figure 7. Spatial profiles of the electric field and the number densities of electrons and ions (total ion density) between the dielectric surface (cathode) and the deflected volume streamer (virtual anode) at the symmetry axis (top) and at the quarter (45° from symmetry axis) of the electrode (bottom) for time $t = t_6$. Data are represented as function of the normal distance from the cathode to the virtual anode.

electron flux are near zero because this instant is before arrival of the streamer head at the represented axial position. With arrival of the streamer ($t = t_1 - 0.1$ ns and $t = t_1$ in figure 5(b)) both rates increase and for later times the radial development of the streamer exhibits similar properties as observed during the axial propagation (cf $t = t_1 + 0.2$ ns).

The results of the present analysis support the assumption that the particular field configuration and source of free electrons determine the direction of the streamer propagation and the increasing electron production rate S_e in radial direction

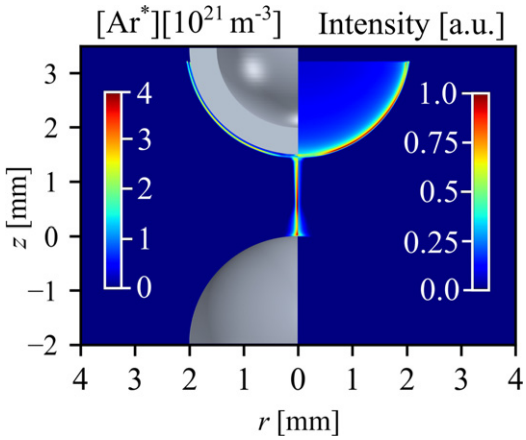

Figure 8. Comparison of non-transformed (left) and Abel-transformed (right) profiles of the excited Ar* states at time $t = t_6$.

around t_1 (cf figure 4) explains the deflection of the volume streamer.

In addition to the inhomogeneous electric field, surface charges play an important role in the surface streamer development and the cathode-layer formation. In order to illustrate this, the spatial distribution of the surface charge density σ along the dielectric boundary (i.e. circular distance on the dielectric, measured from the axis of symmetry of the discharge at the centre of the electrode) is represented in figure 6. It can be seen that the accumulation of surface charges is negligible until the streamer reaches the cathode at t_1. Then, the amount of accumulated surface charges starts to increase near the centre of the electrode around t_2, i.e. when the secondary breakdown at the plasma-surface interface occurs. This increase of the surface charge density can be attributed to the amplification of the ion flux caused by the strong electric field (cf t_2 in figure 4). At the same time the surface charge accumulation leads to a local reduction of the axial electric field, which causes the radial shift of the electric field maximum and triggers the propagation of the surface discharge just above the dielectric. This appears to be related to the findings in [18] for a surface DBD. Note that the cathode layer formation phase appears to be similar to the findings for a metal cathode in [13, 14], where a limited radial expansion of the cathode layer has been observed. Here, the discharge moves along the surface until almost the whole surface is covered, similar to the behaviour observed in the experiment of [33] for a single-filament configuration with hemispherical electrodes. The curved boundary and the virtual anode provided by the deflected volume streamer give enough space for charge generation and thus for the undisturbed development of the discharge along the surface.

As the surface discharge move further along the surface, the accumulated surface charges expand in circular direction on the dielectric surface (t_2–t_6 in figure 6), which causes a continuous drop of the electric field and finally the decay of the discharge.

It is interesting to note that after passing of the surface discharge, the cathode region resembles that of a normal glow discharge, in which the deflected volume streamer acts as a virtual

anode and electrons are emitted from the dielectric cathode due to ion-induced secondary electron emission. This finding is in accordance with [13, 14, 18]. It is illustrated in figure 7, which shows line profiles of the electric field as well as the number densities of electrons and ions between the dielectric surface (cathode) and the outer plasma filament acting as virtual anode. Similar profiles are observed at the symmetry axis ($r = 0$) and at the quarter of the electrode, but the densities of charge carriers are higher near the symmetry axis due to the stronger electric field in that region.

Finally, figure 8 compares the spatial distribution of the Ar^* density at time t_6 to an artificially calculated emission profile, which was obtained from the Ar^* density by Abel transformation using the pyAbel software [37]. This illustrates that the presented modelling results for the species densities cannot directly be compared with data obtained from optical measurements. The line-of-sight integration results in the highest emission signal at the plasma-surface interface while the density has a maximum in the middle of the gap. Furthermore, the distinct features of cathode-layer formation appear to be hidden to a large extend after Abel transformation.

In summary, the appearance of the simultaneous propagation of a volume streamer and development of a surface discharge near the cathode surface in a single-filament DBD in argon is investigated by means of time-dependent, spatially two-dimensional modelling in axisymmetric geometry. The analysis shows that the primary propagation of the volume streamer across the dielectric surface results from the strong radial component of the electric field, which is mainly caused by the electrode configuration and broadening of the streamer when it approaches the surface. The development of the surface discharge is governed by secondary electron emission and the surface charges accumulated on the dielectric. Furthermore, by analysing the electron number density profiles, and electron production and loss rates, it is confirmed that the appearance of a local maximum in the current can be attributed to the arrival of the streamer at the cathode surface. It is shown that this process is not instantaneous, and occurs slowly due to balancing of the electron production and loss rates. In conclusion, the local maximum of the electric current can be used for reliable estimation of the time of the streamer arrival at the cathode surface, which can be further used for the correlation of optical and electrical measurements.

Acknowledgments

This work was funded by the Deutsche Forschungsgemeinschaft (DFG, German Research Foundation)—project number 407462159. The authors thank T Hoder and H Höft for valuable comments and suggestions.

Data availability statement

The data that support the findings of this study are openly available at the following URL/DOI: 10.34711/inptdat.530 [38].

ORCID iDs

Aleksandar P Jovanović https://orcid.org/0000-0002-7104-6466
Detlef Loffhagen https://orcid.org/0000-0002-3798-0773
Markus M Becker https://orcid.org/0000-0001-9324-3236

References

[1] Kogelschatz U 2003 *Plasma Chem. Plasma Process.* **23** 1–46
[2] Brandenburg R 2017 *Plasma Sources Sci. Technol.* **26** 053001
[3] Massines F, Sarra-Bournet C, Fanelli F, Naudé N and Gherardi N 2012 *Plasma Process. Polym.* **9** 1041–73
[4] Gibalov V I and Pietsch G J 2000 *J. Phys. D: Appl. Phys.* **33** 2618–36
[5] Merbahi N, Sewraj N, Marchal F, Salamero Y and Millet P 2004 *J. Phys. D: Appl. Phys.* **37** 1664
[6] Brandenburg R, Wagner H-E, Morozov A M and Kozlov K V 2005 *J. Phys. D: Appl. Phys.* **38** 1649
[7] Kozlov K V and Wagner H-E 2007 *Contrib. Plasma Phys.* **47** 26–33
[8] Starikovskii A Y, Nikipelov A A, Nudnova M M and Roupassov D V 2009 *Plasma Sources Sci. Technol.* **18** 034015
[9] Soloviev V R and Krivtsov V M 2009 *J. Phys. D: Appl. Phys.* **42** 125208
[10] Hoder T, Brandenburg R, Basner R, Weltmann K-D, Kozlov K V and Wagner H-E 2010 *J. Phys. D: Appl. Phys.* **43** 4009
[11] Hoder T, Loffhagen D, Wilke C, Grosch H, Schäfer J, Weltmann K-D and Brandenburg R 2011 *Phys. Rev.* E **84** 046404
[12] Höft H, Becker M M and Kettlitz M 2018 *Plasma Sources Sci. Technol.* **27** 03LT01
[13] Braun D, Gibalov V and Pietsch G 1992 *Plasma Sources Sci. Technol.* **1** 166–74
[14] Steinle G, Neundorf D, Hiller W and Pietralla M 1999 *J. Phys. D: Appl. Phys.* **32** 1350–6
[15] Yurgelenas Y V and Wagner H-E 2006 *J. Phys. D: Appl. Phys.* **39** 4031–43
[16] Papageorghiou L, Panousis E, Loiseau J F, Spyrou N and Held B 2009 *J. Phys. D: Appl. Phys.* **42** 105201
[17] Celestin S, Bonaventura Z, Guaitella O, Rousseau A and Bourdon A 2009 *Eur. Phys. J. Appl. Phys.* **47** 2810
[18] Gibalov V I and Pietsch G J 2012 *Plasma Sources Sci. Technol.* **21** 024010
[19] Becker M M, Hoder T, Brandenburg R and Loffhagen D 2013 *J. Phys. D: Appl. Phys.* **46** 355203
[20] Callegari T, Bernecker B and Boeuf J P 2014 *Plasma Sources Sci. Technol.* **23** 054003
[21] Xu Y, Wang J, Li J, Lei B, Tang J, Wang Y, Li Y, Zhao W and Duan Y 2017 *Phys. Plasmas* **24** 043507
[22] Babaeva N Y, Tereshonok D V and Naidis G V 2016 *Plasma Sources Sci. Technol.* **25** 044008
[23] Kourtzanidis K, Dufour G and Rogier F 2021 *J. Phys. D: Appl. Phys.* **54** 045203
[24] Kogelschatz U 2002 *IEEE Trans. Plasma Sci.* **30** 1400–8
[25] Černák M, Hoder T and Bonaventura Z 2020 *Plasma Sources Sci. Technol.* **29** 013001
[26] Jánský J, Bessiéres D, Brandenburg R, Paillol J and Hoder T 2021 *Plasma Sources Sci. Technol.* **30** 105008
[27] Sharma A, Levko D and Raja L L 2016 *Phys. Plasmas* **23** 103501

[28] Meyer H K H, Marskar R, Gjemdal H and Mauseth F 2020 *Plasma Sources Sci. Technol.* **29** 115015
[29] Dubinova A, Trienekens D, Ebert U, Nijdam S and Christen T 2016 *Plasma Sources Sci. Technol.* **25** 055021
[30] Li X, Sun A, Zhang G and Teunissen J 2020 *Plasma Sources Sci. Technol.* **29** 065004
[31] Sigeneger F and Loffhagen D 2016 *Plasma Sources Sci. Technol.* **25** 035020
[32] COMSOL Multiphysics® 2020 *Version. 5.6* (Stockholm, Sweden: COMSOL AB) www.comsol.com
[33] Kloc P, Wagner H-E, Trunec D, Navrátil Z and Fedoseev G 2010 *J. Phys. D: Appl. Phys.* **43** 5205
[34] Odrobina I and Černák M 1992 *Czech. J. Phys.* **42** 303–15
[35] Odrobina I and Černák M 1995 *J. Appl. Phys.* **78** 3635–42
[36] Synek P, Zemánek M, Kudrle V and Hoder T 2018 *Plasma Sources Sci. Technol.* **27** 045008
[37] Hickstein D D, Gibson S T, Yurchak R, Das D D and Ryazanov M 2019 *Rev. Sci. Instrum.* **90** 065115
[38] Jovanović A P, Loffhagen D and Becker M M 2022 *INPTDAT* https://doi.org/10.34711/inptdat.530